AIP Advances

Rapid optical determination of topological insulator nanoplate thickness and oxidation

Cite as: AIP Advances **7**, 015114 (2017); https://doi.org/10.1063/1.4973403
Submitted: 18 November 2016 • Accepted: 12 December 2016 • Published Online: 30 January 2017

Fan Yang, Mariana Sendova, Robin B. Jacobs-Gedrim, et al.

ARTICLES YOU MAY BE INTERESTED IN

Reversible phase-change behavior in two-dimensional antimony telluride (Sb_2Te_3) nanosheets
Applied Physics Letters **112**, 133101 (2018); https://doi.org/10.1063/1.5013099

Micro-Raman spectroscopy of mechanically exfoliated few-quintuple layers of Bi_2Te_3, Bi_2Se_3, and Sb_2Te_3 materials
Journal of Applied Physics **111**, 054305 (2012); https://doi.org/10.1063/1.3690913

A two-step process for growth of highly oriented Sb_2Te_3 using sputtering
AIP Advances **6**, 045220 (2016); https://doi.org/10.1063/1.4948536

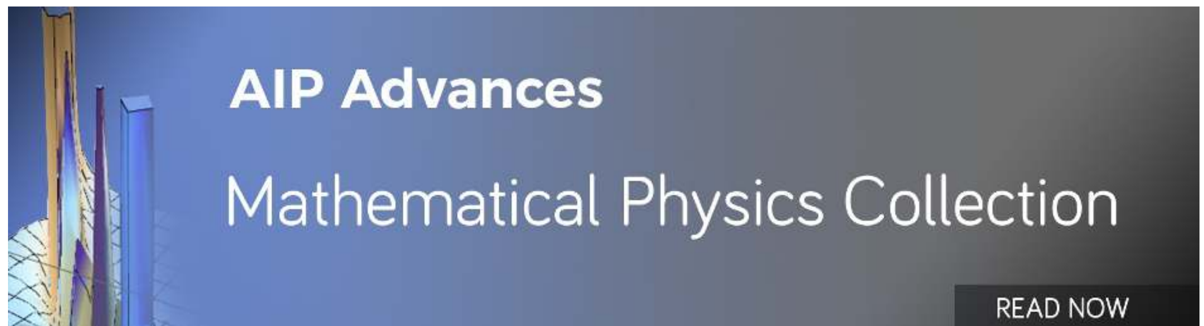

© 2017 Author(s).

AIP Publishing

CrossMark click for updates

Rapid optical determination of topological insulator nanoplate thickness and oxidation

Fan Yang,[1] Mariana Sendova,[2] Robin B. Jacobs-Gedrim,[1] Eui Sang Song,[1] Avery Green,[1] Peter Thiesen,[3] Alain Diebold,[1] and Bin Yu[1,a]
[1]*College of Nanoscale Science and Engineering, State University of New York, 253 Fuller Rd., Albany, NY 12203, USA*
[2]*New College of Florida, 5800 Bay Shore Rd., Sarasota, FL 34243, USA*
[3]*Accurion Gmbh, Stresemannstraße 30, 37079 Göttingen, Germany*

(Received 18 November 2016; accepted 12 December 2016; published online 30 January 2017)

The stability of 2D antimony telluride (Sb_2Te_3) nanoplates in ambient conditions is elucidated. These materials exhibit an anisotropic oxidation mode, and CVD synthesized samples oxidize at a much faster rate than exfoliated samples investigated in previous studies. Optical measurement techniques are introduced to rapidly measure the oxidation modes and thickness of 2D materials. Auger characterization were conducted to confirm that oxygen replaces tellurium as opposed to antimony under ambient conditions. No surface morphology evolution was detected in AFM before and after exposure to air. These techniques were employed to determine the origin of the thickness dependent color change effect in Sb_2Te_3. It is concluded that this effect is a combination of refractive index change due to oxidation and Fresnel effects. © *2017 Author(s). All article content, except where otherwise noted, is licensed under a Creative Commons Attribution (CC BY) license (http://creativecommons.org/licenses/by/4.0/).* [http://dx.doi.org/10.1063/1.4973403]

INTRODUCTION

Two-dimensional (2D) binary sesquichalcogenides are viable material platforms for future flexible and low power nanodevices.[1–4] The unique properties of nanoscaled chalcogenide materials may enable future technologies such as integrated photonics and spintronics as well as providing a platform for fundamental research on the physics of low dimensional condensed matter systems.[5,6] Sb_2Te_3, Bi_2Se_3, and Bi_2Te_3 are topological insulators with a single Dirac cone in their interface with an insulator, vacuum, or superconductor.[7,8] These materials also exhibit spin-momentum locking of the helical Dirac electrons.[9] While 2D binary sesquichalcogenides are of considerable scientific and technological interest, conflicting reports of their ambient stability under a variety of sample preparation methods exist.[10]

As the chemical purity of binary sesquichalcogenide nanostructures is so critical for technological application, a facile method for rapidly determining the chemical composition of these nanostructures is required, we previously did for graphene observation.[11] Optical characterizations are one of the most rapid methods for identifying chemical composition.[12] If it is possible to visualize (in the optical microscope) the effects of contamination, processing problems can be rapidly identified and eliminated. Here it is shown that it is possible to observe the oxide formation in sub-20 nm thick Sb_2Te_3 nanoplates on 100 nm thick SiO_2 in the optical microscope due to a change in the refractive indices of the material and Fresnel effects. As color is subjective to the human eye, quantitative UV-Vis-NIR microspectrophotometer measurements are used to determine the reflected spectra from the nanoplates. In addition, imaging ellipsometry is implemented to determine optical constants. Furthermore, Auger electron spectroscopy is utilized to verify that the changes in optical properties arise from oxidation. This investigation clarifies the origin of thickness-and chemistry-dependent

[a]Corresponding Author: byu@sunypoly.edu

 © Author(s) 2017

changes in the optical properties of ultra-thin Sb_2Te_3 nanoplates and allows for the rapid identification of thickness and chemical purity through optical means.

A single step CVD growth of Sb_2Te_3 nanoplates was performed as our previous reports.[13] A 100 nm SiO_2/Si target substrate was placed 5 cm from edge of the furnace, and source powder was placed in the furnace center. The chamber was first evacuated starting by evacuated to 15 mTorr vacuum for 30 minutes. The chamber conditions were set at 550° C, 7 minutes, and 100 standard cubic centimeters (SCCM) Ar flow. Due to the flow of carrier gas and evaporated material, the chamber pressure raised to ~680 mTorr during evaporation. Since many nanoplates were characterized, we marked the as-grown nanoplate sample name as SD#growth number#-#nanoplate thickness#. The first growth results optical microscope image is shown in Fig. 1a. Hexagonal and triangular nanoplates with varying colors were obtained through deposition process. The nanoplate in the left image ~ 8 nm/8 quintuple layers thick (e.g. sample name SD1-8), and nanoplates in the right image are ~13 quintuple layers thick (sample SD1-13) and 10 quintuple layers thick (sample SD1-10) respectively. We assumed that the different color reflects from these thin flakes are due to Fresnel effect in different thickness nanoplates on SiO_2/Si substrate. AFM was conducted to determine the nanoplate thickness, as shown in Fig. 1b and 1c. The nanoplates are observed to have hexagonal and triangular shape with lateral dimensions of 10-30 µm across, the nanoplates' height ranges from 6 nm up to several hundred nanometers thickness. The surface of the nanoplates are atomically smooth, indicating complete growth to the van der Waal's gap. It is worth noting that, in this optical image, brown color indicates nanoplates thickness between 6 nm to 15 nm, and the white color indicates a thickness of over 25 nm and black for vertical growth nanoplates.

By qualitatively comparing the optical images and the AFM data, it is clear that there is a physical relationship between layer thickness and color change as seen in Fig. 1c. As thickness is decreased the color of the nanoplates transitions from white to red and orange, and then finally on the thinnest plate, is a blue color closely matching that of the SiO_2/Si substrate, which may indicate that the

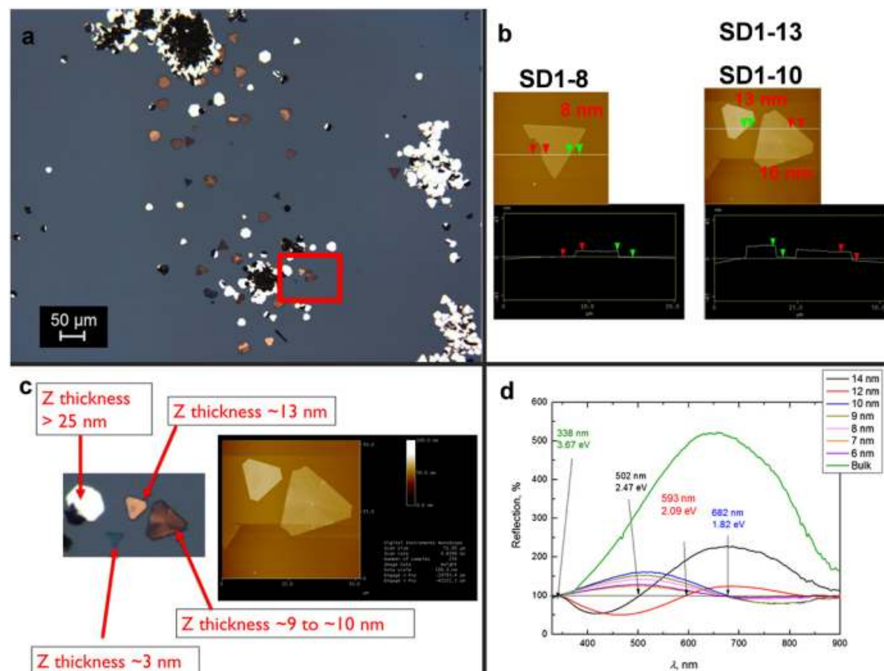

FIG. 1. a) Optical microscope image of Sb_2Te_3 nanoplates taken immediately after the growth process; b) AFM images and line scans of the nanoplates outlined in red (sample SD1-8, SD1-10, and SD1-13); c) Comparison of the optical image to the AFM image demonstrating some qualitative link between nanoplate thickness and color (sample SD1-3, SD1-13, and SD1-30); d) UV-Vis-NIR reflectance spectra of nanoplates with varying thicknesses. Bulk indicates a very thick nanoplate (>200 nm), above the reliable step height measurement of the AFM, that was used to as an indicator of the bulk reflection properties of the material.

nanoplate is transparent. It has been suggested in literature that this color change is due to quantum-confinement.[13] It can be observed that the color change of the material is dramatic as thickness is minimized in Fig. 1c. Color of SD1-3 nanoplate is blue, while SD1-9 and SD1-13 is brown. And nanoplates above 25 nm in thickness seems to reflect far more light than other ultrathin nanoplates to exhibit a shining white color (e.g. SD1-30 in Fig. 1c). It has been suggested theoretically and demonstrated experimentally that the topological insulator state of Sb_2Te_3 only exists in films above 2 nm in thickness as the surface state at the top and bottom of the film interfere destructively in the 2D limit.[14,15]

While a qualitative relationship between the thickness and color of the nanoplates may be observed merely with optical microscopy, lighting conditions, and the subjective nature of color in general, requires that a quantitative method be employed to determine the exact reflection spectrum of individual nanoplates. In order to get rid of noises mentioned above, we employed Craic Microspectrophotometer with a 1 x1 µm collection area, as illustrated in Fig. 1d. The UV-Vis-NIR data shows a reduction in the peak reflection value from the bulk sample down to 12 nm (SD1-12). However, there is an inversion in the reflection signal below 12 nm. It is also worth noting that at this point, the nanoplates had spent a considerable amount of time in ambient conditions, and their color as observed in the optical microscope was changing. To determine if this was an expected result, a simulation of the reflection was performed using bulk n and k values from the literature and simulated substrate of 100 nm SiO_2 and Si to match the experiment as shown in Fig. 2.[16] Seen from those curves, the reflection percentage as compared to substrate increases as number of nanoplates layers increases. No reverse reflection was obtained according to calculation results.

The discrepancy between the theoretically predicted and experimentally observed reflection results was further investigated with the use of an EP4 imaging Ellipsometer, as shown in Fig. 3. We chose two nanoplates SD1-10 and SD1-12 with 10 nm and 12 nm thickness, respectively. And it is seen that S1-12 nanoplate showed brown color while SD1-10 nanoplate showed blue color from optical microscope in Fig 3a. The EP4 uses null ellipsometry in an imaging mode which gives it a surface lateral resolution of 1 µm. The amplitude ratio ψ and phase difference Δ are measured by reflecting light off of the nanoplate and measuring the elliptically polarized light. A Kramer-Kronig model taking into account the Si substrate, 100 nm SiO_2 layer, and the AFM measured thickness of the Sb_2Te_3 nanoplates is used to extract the optical constants n and k.[17]

The inversion of the optical constant slope with respect to wavelength revealed by ellipsometry, and the time dependent color change indicates that this is due to a chemical change in the nanoplates under ambient conditions. The likely candidate is oxidation. To verify this assumption Auger electron spectroscopy was employed as shown in Fig. 3d. Auger electron spectroscopy is a surface sensitive technique with a sampling depth in Sb_2Te_3 of 1 ∼ 5 nm, smaller than the ∼10 nm thickness of the nanoplates such that no signal from the SiO_2 substrate was present. Oxygen was a dominant peak on

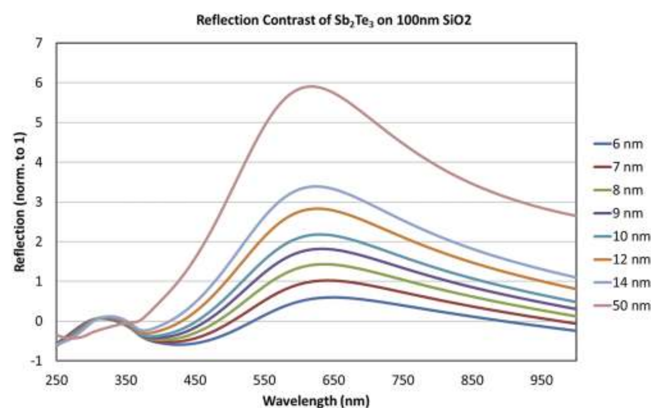

FIG. 2. Simulation of reflection of a thin film of Sb_2Te_3 on 100 nm SiO_2/Si substrate. Note that no inversion of the reflection spectra is expected due to Fresnel effects down to 6 nm thickness.

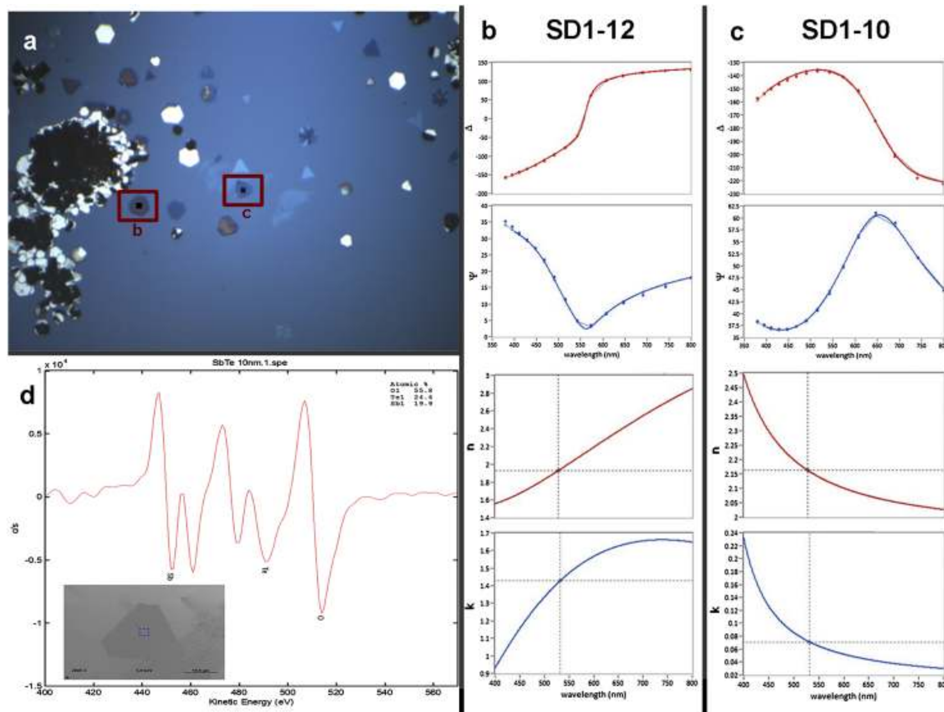

FIG. 3. a) Color changing nanoplates. Black dots indicate the location of the UV-Vis-NIR data taken of the SD1-12 nanoplate in the bottom image of the figure, and the SD1-10 nanoplate in the top figure; b) Ellipsometry data taken from the SD1-12 nanoplate; c) Ellipsometry data taken from the SD1-10 nanoplate; d) Auger electron spectrum of single SD1-10 Sb_2Te_3 nanoplate. Oxygen is a dominant peak in the analysis.

the SD1-10 nanoplate, which explains the color change as a switch from stoichiometric Sb_2Te_3 to $Sb_2Te_{1-x}O_x$.

After observing the color change phenomenon, the same CVD process for Sb_2Te_3 nanoplates deposition was repeated, and a systematic study on oxidation rate and reflection/morphology evolution for deposited Sb_2Te_3 was performed. We systematically characterized two ultrathin nanoplates with 27 nm and 8 nm in thickness named SD2-27 and SD2-8, respectively. In addition, mechanical exfoliation method was conducted to obtain Sb_2Te_3 nanoflakes on same wafer substrate with higher crystallinity. And we marked two specific ultrathin nanoflakes as SM2#1 and SM2#2. Fig. 4 illustrates Auger signals and trending curves on oxidation evolution for SM2#1, SM2#2, SD2-27, and SD2-28 samples. High resolution Auger analysis of the Sb, Te, and O element peaks ranging from 400 eV to 600 eV, is shown in Fig. 4a, 4c, 4e, and 4g, respectively. It is clearly observed from curves of mechanical exfoliation samples that, as exposing time increases, the percentage of antimony and oxidation signal increases while the tellurium signal decreases. However, for CVD nanoplates, more peak shifting occurred, making it hard to intuitively detect the elemental percentage trend. To address this, the elemental percentage was extracted from raw data and a relationship between elemental percentage and exposure duration was obtained, as shown in Fig. 4b, 4d, 4f, and 4h, respectively. A similar elemental percentage trending was observed: 1. Initial oxygen percentage of deposited samples is ~ 20% higher than exfoliated ones; 2. The percentage of antimony stays relatively constant during under air exposure, while the percentage of tellurium decreases significantly, replaced by increasing oxygen; 3. The oxygen percentage for both deposited and exfoliated samples increases fast in the first few days, and become stable or increases very slow after 3 ~ 6 days. And after 15 ~ 20 days, the ratio of Sb: Te: O for exfoliated nanoplates was ~ 7:8:10, while for CVD samples was ~ 3:2:5. It is worth noting that no obvious color change happened under optical microscope during nearly a month's measurement. We believed that oxidation will increase slowly further to replace more tellurium atoms and change the color of nanoplates as the trend is increasing still at the end of measurements; 4. In over 15 days' Auger measurement, ~ 15% decrease of tellurium percentage

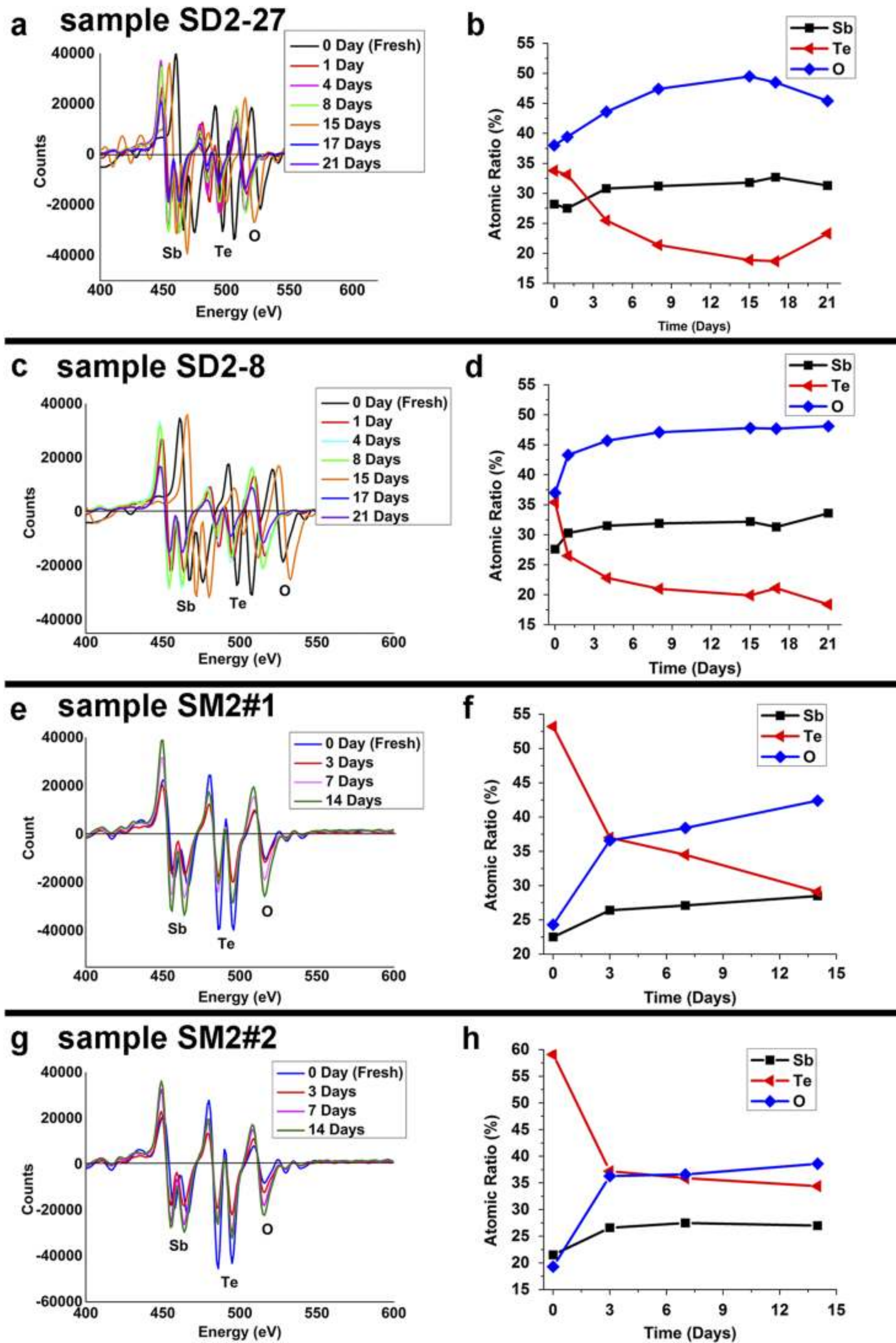

FIG. 4. High-res Auger mapping of Sb, Te, and O element ranging from 400 eV to 600 eV for deposited and mechanical exfoliated samples a) SD2-27 nanoplate; c) SD2-8 nanoplate; e) SM2#1; g) SM2#2. b), d), f), and h) Right four image shows corresponding extracted data on relationship between elemental percentage and air exposure duration for all four samples, respectively.

was detected over deposited samples, while ~ 25% decrease for exfoliated samples. But because of higher initial tellurium percentage, final oxidation state of deposited nanoplates is higher overall; 5. For different thickness of deposited sample and exfoliated samples, not much difference in the oxidation process were detected. It is noted that the Auger measurement spot is at center of the nanoplates. From the discussion, it is likely that oxygen element replaces tellurium during air exposure.

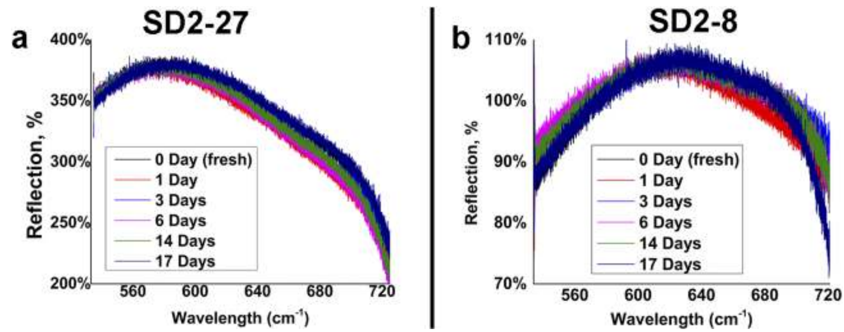

FIG. 5. Reflection curves of a) SD2-27 nanoplate and b) SD2-8 nanoplate at different air exposure time for wavelengths of light ranging from 535 nm to 900 nm. SiO_2/Si substrate curve was also performed as reference sample.

In addition to Auger analysis, optical reflection and AFM were also conducted to check surface status and morphology evolution of deposited Sb_2Te_3 nanoplates. Fig. 5a and 5b shows relationship between normalized optical reflection and visible/near infrared wavelength of SD2-27 and SD2-8 nanoplates, respectively, with different durations of exposure to ambient condition. It is seen from reflection curves that, as thickness increase from 8 nm (SD2-8 sample) to 27 nm (SD2-27 sample), reflection also increases, the same as calculated results in Fig. 2. Other than intensity, an obvious red shift of reflection curve was detected of thinner SD2-8 nanoplate than thicker SD2-27 nanoplate. The reflection shift results illustrated for second deposition process is the same as first growth in Fig. 1d. Besides, with increasing air exposure time, a slightly red shifted can be seen for each sample, respectively.

Fig. 6a and 6b exhibit AFM measurement results of SD2-8 and SD2-27 samples, respectively. No significant difference in morphology before and after air exposure was observed. The extracted

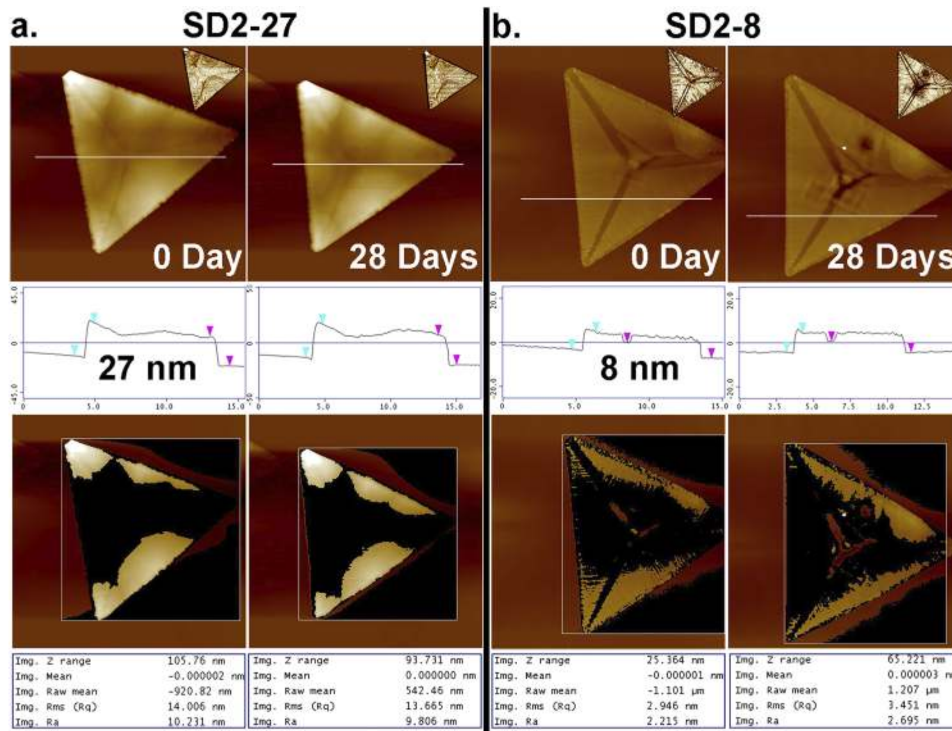

FIG. 6. AFM images of deposition Sb_2Te_3 samples a) SD2-27 nanoplate and b) SD2-8 nanoplate analyzed by Auger spectroscopy above: first row performs height mapping with inset; second row depicts extracted line scan for nanoplates; third row and fourth row shows mean roughness of the image and the sample, where black region indicates atomic smoothness.

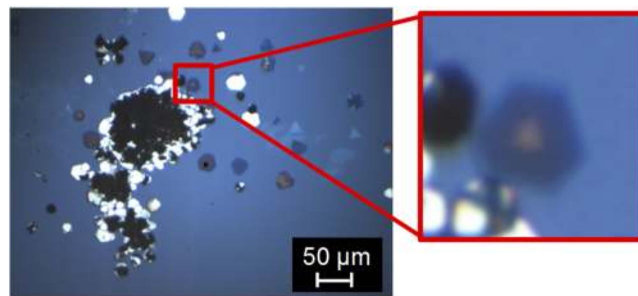

FIG. 7. Magnified optical image of a $Sb_2Te_{1-x}O_x$ in which anisotropic oxidation may be observed. The center of the nanoplate appears orange, indicating there is a region of Sb_2Te_3 whereas the edges appear dark blue indicating that these regions have oxidized. The oxidation perpendicular to the sample surface is orders of magnitude slower than oxidation in the directions parallel to the sample surface.

scanned lines depicted at second row of Fig. 6 are similar for both CVD samples with different air exposure time. It is noted that, from AFM analysis, a clear spot and square line region was observed near center of SD2-8 nanoplates, as shown in first row of Fig. 6b. This is the sign of damage caused by laser based Auger characterization method. Image roughness data and surface mapping indicates stable structure during the slow oxidation process. It is likely that oxygen replaced tellurium atoms in the unit cell position of original crystal structure.

According to discussion above, it is unfortunate that the observed color change is due to Fresnel effects and oxidation alone, in comparison to some exotic quantum confinement effects as implied by other studies,[18] the optical techniques employed here provided a valuable tool in terms of rapidly addressing questions regarding the chemical purity of Sb_2Te_3 nanoplates. It is possible, for instance, to determine whether a thin nanoplate is of pure quality simply by observing its color in the optical microscope, or in the UV-Vis-NIR if a quantitative answer is required. Additionally, an anisotropic oxidation mode is observed in this experiment. Take, for instance the SD1-20 nanoplate with 20 nm in thickness shown in Fig. 7.

The nanoplate shows oxidation in all directions, but oxidation in the directions parallel to the a and b axes are many orders of magnitude faster than oxidation parallel with the c axis. The AFM images as shown in Fig. 1 indicate that the nanoplates are a few nanometers thick and atomically smooth. If an isotropic oxidation rate were assumed, the nanoplate would completely oxidize from top to bottom 20 nm thickness (SD1-20 nanoplate) much faster than from the edges toward the center (~10 µm in diameter), as complete top to bottom oxidation is not observed, this assumption must be false. The anisotropic oxidation is therefore attributed to dangling bonds at the edges of the nanoplate, and the lack thereof on the self-terminated (0001) surface.[1]

EXPERIMENTAL METHODS

A single step CVD growth of Sb_2Te_3 nanoplates was performed. A 100 nm SiO_2/Si target substrate was placed 5 cm from edge of the furnace, and source powder was placed in the furnace center. The chamber was first evacuated starting by evacuated to 15 mTorr vacuum for 30 minutes. The chamber conditions were set at 550° C, 7 minutes, and 100 SCCM Ar flow. Due to the flow of carrier gas and evaporated material, the chamber pressure raised to ~680 mTorr during evaporation. A Craic Instruments Microspectrophotometer was employed for UV-Vis-NIR measurements. Optical constant measurements were performed with a Accurion Gmbh EP4 imaging Ellipsometer. AFM measurements were done with a Bruker Dimension 3100 AFM. AES measurements were performed with a Perkin-Elmer Model 680 Auger spectrometer.

[1] Q. H. Wang, K. Kalantar-Zadeh, A. Kis, J. N. Coleman, and M. S. Strano, Nature Nanotechnology **7**, 699 (2012).
[2] F. H. L. Koppens, T. Mueller, P. Avouris, A. C. Ferrari, M. S. Vitiello, and M. Polini, Nature Nanotechnology **9**, 780 (2014).
[3] B. Radisavljevic, A. Radenovic, J. Brivio, V. Giacometti, and A. Kis, Nature Nanotechnology **6**, 147 (2011).
[4] A. K. Geim and I. V. Grigorieva, Nature **499**, 419 (2013).
[5] X. Tao and Y. Gu, Nano Letters **13**, 3501 (2013).

[6] D. Kong, J. C. Randel, H. Peng, J. J. Cha, S. Meister, K. Lai, Y. Chen, Z.-X. Shen, H. C. Manoharan, and Y. Cui, Nano Letters **10**, 329 (2009).
[7] H. Zhang, C.-X. Liu, X.-L. Qi, X. Dai, Z. Fang, and S.-C. Zhang, Nature Physics **5**, 438 (2009).
[8] W. Dang, H. Peng, H. Li, P. Wang, and Z. Liu, Nano Letters **10**, 2870 (2010).
[9] D. Hsieh, Y. Xia, D. Qian, L. Wray, J. H. Dil, F. Meier, J. Osterwalder, L. Patthey, J. G. Checkelsky, N. P. Ong *et al.*, Nature **460**, 1101 (2009).
[10] V. V. Atuchin, V. A. Golyashov, K. A. Kokh, I. V. Korolkov, A. S. Kozhukhov, V. N. Kruchinin, S. V. Makarenko, L. D. Pokrovsky, I. P. Prosvirin, K. N. Romanyuk *et al.*, Crystal Growth and Design **11**, 5507 (2011).
[11] F. Yang, Y. Liu, W. Wu, W. Chen, L. Gao, and J. Sun, Nanotechnology **23**(47), 475705 (2012).
[12] J. A. Soares, *Practical Materials Characterization* (Springer, 2014), pp. 43–92.
[13] F. Yang, R. B. Jacobs-Gedrim, M. Shanmugam, N. Jain, M. T. Murphy, E. S. Song, and B. Yu, RSC Advances **5**(73), 59320–59325 (2015).
[14] A. Vargas, S. Basak, F. Liu, B. Wang, E. Panaitescu, H. Lin, R. Markiewicz, A. Bansil, and S. Kar, ACS Nano **8**, 1222 (2014).
[15] Y.-Y. Li, G. Wang, X.-G. Zhu, M.-H. Liu, C. Ye, X. Chen, Y.-Y. Wang, K. He, L.-L. Wang, X.-C. Ma *et al.*, Advanced Materials **22**, 4002 (2010).
[16] W. Richter, A. Krost, U. Nowak, and E. Anastassakis, Zeitschrift Für Physik B Condensed Matter **49**, 191 (1982).
[17] G. B. Arfken, *Mathematical Methods for Physicists* (Academic Press, 2013).
[18] A. Vargas, F. Liu, and S. Kar, "Giant enhancement of light emission from nanoscale Bi2Se3," Applied Physics Letters **106**, 243107 (2015).